
CATS: Enhancing Multivariate Time Series Forecasting by Constructing Auxiliary Time Series as Exogenous Variables

Jiecheng Lu¹ Xu Han² Yan Sun¹ Shihao Yang¹

Abstract

For Multivariate Time Series Forecasting (MTSF), recent deep learning applications show that univariate models frequently outperform multivariate ones. To address the deficiency in multivariate models, we introduce a method to Construct Auxiliary Time Series (CATS) that functions like a 2D temporal-contextual attention mechanism, which generates Auxiliary Time Series (ATS) from Original Time Series (OTS) to effectively represent and incorporate inter-series relationships for forecasting. Key principles of ATS—continuity, sparsity, and variability—are identified and implemented through different modules. Even with a basic 2-layer MLP as core predictor, CATS achieves state-of-the-art, significantly reducing complexity and parameters compared to previous multivariate models, marking it an efficient and transferable MTSF solution.

1. Introduction

Time series forecasting plays a pivotal role in domains like finance, health, and traffic, focusing on predicting future data based on historical records (Kaastra & Boyd, 1996; Nihan & Holmesland, 1980; Sun & Yang, 2023; Ma et al., 2022). The complexity increases in multivariate time series forecasting (MTSF), where understanding the interdependencies among multiple series is needed for accuracy. Effectively modeling these relationships is key to overcoming challenges such as overfitting, thus enhancing the reliability of predictions.

Recent research in MTSF with deep learning methods reveals a counter-intuitive trend: univariate models, which ignore inter-series relationships, often outperform their multivariate counterparts (Zeng et al., 2023; Nie et al., 2022; Lu et al., 2023). This phenomenon suggests two potential issues: 1) The real-world benchmark datasets selected

for study may inherently possess weak inter-series relationships; 2) Previous models may lack the proper structure needed to effectively capture inter-series relationships. This inadequacy often leads to overfitting or fitting of wrong patterns. Moreover, in situations where intra-series (temporal) relationships dominate, attempts to incorporate inter-series information may inadvertently disrupt the learning of temporal dynamics, resulting in the multivariate underperformance. This highlights the need for models that can balance and harness both types of relationships in MTSF.

In this paper, we introduce an approach to effectively capture the two types of relationships in MTSF: Constructing Auxiliary Time Series (CATS). This approach empowers a time series predictor to handle diverse strengths of multivariate relationships, without altering its model architecture, even when the predictor is a structurally simple univariate model. CATS operates by generating Auxiliary Time Series (ATS) based on the Original Time Series (OTS), serving as exogenous variables to represent the inter-series relationships. By predicting these exogenous time series, CATS finds and incorporates multivariate information to the prediction of OTS, thereby boosting overall performance.

We define ATS as the intermediary time series that are derived from the OTS input, reside in the same temporal domain as the original series. ATS can refine the univariate forecasting results with inter-series information. There are three key principles of ATS: continuity, sparsity, and variability. These principles are crucial when the inter-series relationships are weak, complex, or challenging to learn. ATS are constructed with these three principles using specific neural network structures, gating operations, and loss terms. This construction allows the ATS to effectively extract and represent multivariate relationships.

1.1. Basic Intuition: How CATS Works?

We present an intuitive example to demonstrate the efficacy and working mechanism of CATS. We apply the simplest form of ATS constructor – identity mapping – and use a basic independent linear predictor for prediction. Despite the ATS merely replicates the OTS, it remarkably transforms a univariate model into a model capable of capturing challenging multivariate relationships, through a mechanism similar

¹Georgia Institute of Technology ²Amazon Web Services. Correspondence to: Jiecheng Lu <jlu414@gatech.edu>, Shihao Yang <shihao.yang@isye.gatech.edu>.

to 2D temporal-contextual attention.

The example is a simple shifting problem introduced by (Lu et al., 2023) using a *Multi* dataset, where the best solution is a copy-paste operation. However, most multivariate models struggle due to challenges in timestep mixing as well as managing relationship across different time steps of multivariate series (see the *Multi* results in Table 1 and 7).

Shifting Problem Consider a scenario with two time series: a random walk series X^1 , and another series X^2 derived by shifting X^1 backward by 96 steps. We set up a MTSF problem where the inputs comprises 144 steps (denoted as X_I^1 and X_I^2), and the goal is to predict the subsequent 48 steps (denoted as X_P^1 and X_P^2). For each series considered independently, the best univariate predictor \hat{X}_{Uni}^1 and \hat{X}_{Uni}^2 is a repetition of their last input value $X_I^{(144),1}$ and $X_I^{(144),2}$, respectively. However, when these series are considered together, an optimal predictor for X^2 would copy-paste steps 49 to 96 from X^1 , denoted as $\hat{X}_P^2 = X_P^2 = X_I^{(49:96),1}$.

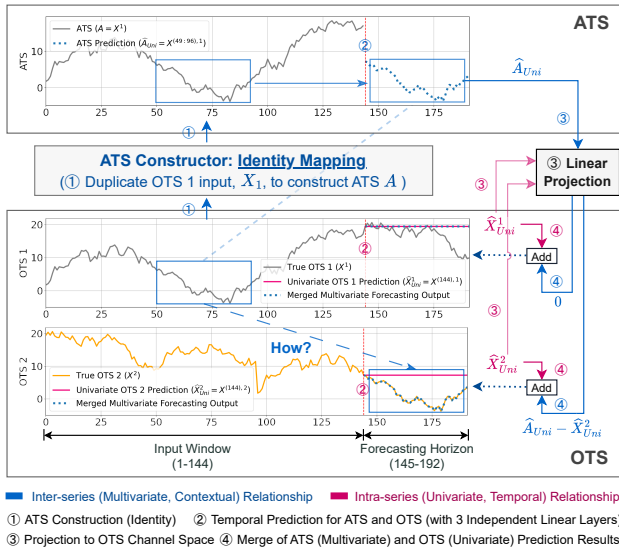


Figure 1. The Basic CATS Solution of the Shifting Problem

Using the CATS structure, as shown in Figure 1, we initially duplicate the first series to create an ATS, denoted as $A_I = X_I^1$. For the prediction, we use independent linear layers for each of X^1 , X^2 , and A . The best independent predictors for X^1 and X^2 will remain as their last values. However, the ATS’s linear layer operates differently. Let the weight matrix for this layer be denoted by $W \in \mathbb{R}^{48 \times 144}$. When W is structured such that its entries $W_{[:,49:96]} = I$ and 0 otherwise, this layer effectively “transports” the steps 49 to 96 of the first series to the ATS’s output with $\hat{A}_{Uni} = WA_I = \hat{X}_I^{(49:96),1}$. Subsequently, a linear mapping then “transports” this segment from the ATS’s output to the OTS output domain, making $\hat{X}_P^2 = X_I^{(49:96),1}$.

In this simplified setting, even without complex network structure, CATS adaptively learns the inter-series relationship. This demonstrates CATS as an adaptive mechanism that focuses on specific regions of the OTS, summarize the inter-series information in ATS, and effectively transfers it from the input to the output domain, finally integrating it into the OTS output through projection.

The shifting problem example shows that CATS can be viewed as an adaptive 2-dimensional temporal and series-wise attention mechanism: it dynamically focuses on specific regions of the OTS, and extract the inter-series information into ATS, effectively transfers this information from the input to the output time domain via the main predictor. Ultimately, it merges the gathered information into the OTS output using a projection, as illustrated in Figure 2. For more complicated time series, CATS will expand the number of ATS and use general ATS constructors.

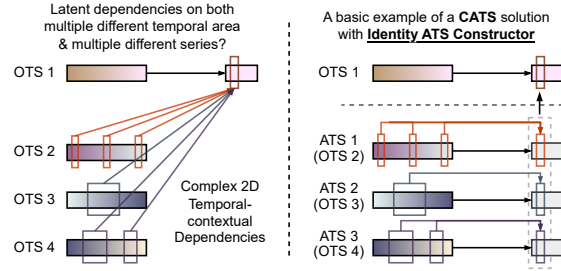


Figure 2. 2D Temporal-contextual Attention-like Mechanism

The key contributions of this paper can be summarized as:

- 1) We introduce the Constructing ATS (CATS) approach based on the multivariate OTS, which empowers time series predictors with the ability of efficient capturing the inter-series relationships with a 2D attention-like mechanism.
- 2) We identify three key principles essential for the efficacy of ATS: continuity, sparsity, and variability, and design specific modules that enforce these principles.
- 3) We propose various types of ATS constructors, offering adaptability to general MTSF datasets, demonstrating the versatility of CATS in handling diverse MTSF challenges.

2. Related Works

Time series forecasting models have been extensively studied in traditional statistical literature (Box et al., 1974; Holt, 2004; Sims, 1980). The advent of deep learning methods has provided time series forecasting with enhanced fitting capabilities, especially those based on RNN and CNN (Hochreiter & Schmidhuber, 1997; Wen et al., 2017; Rangapuram et al., 2018; Salinas et al., 2020; Qin et al., 2017; Borovykh et al., 2017; van den Oord et al., 2016), as well as more recent Transformer-based complex MTSF models (Wen

et al., 2022). However, studies have pointed out that simpler univariate models, which ignore the relationships between series, can surpass these complex models (Zeng et al., 2023; Nie et al., 2022). This indicates that previous complex models may not effectively model these relationships.

For MTSF, effectively handling both temporal and contextual dimensions is crucial. Nonetheless, recent complex models are typically driven by 1D temporal attention mechanisms, as seen in LogTrans (Li et al., 2019), Informer (Zhou et al., 2021), Autoformer (Wu et al., 2021), etc, which has been shown to inadequately capture series-wise relationships (Zeng et al., 2023; Lu et al., 2023). Some research also tried to explicitly model series-wise relationships (Liu et al., 2023), but the input temporal embedding diminish the effectiveness with longer input length. Crossformer (Zhang & Yan, 2023) tried to build a 2D attention mechanism, but its performance did not surpass linear univariate models. ARM (Lu et al., 2023) attempted to simulate 2D attention by weighting the results of temporal attention with channel attention scores, but its complexity and reliance on univariate components limit its effectiveness.

3. Method

In MTSF, our primary objective is to forecast the future values of a time series, represented as $\hat{X}_P \in \mathbb{R}^{L_P \times C}$, given its historical data, denoted as $X_I \in \mathbb{R}^{L_I \times C}$. Here, $X \in \mathbb{R}^{L \times C}$ signifies the entire time series, where $L = L_I + L_P$ represents the total length of the series, L_I is the input or lookback window length, L_P is the forecasting horizon, and C indicates the number of input series or channels. In this setting, $X^{(t),i}$ denotes the value at the t -th time step of the i -th series, with $t \in \{1, \dots, L\}$ and $i \in \{1, \dots, C\}$.

Addressing the intricacies of MTSF, we introduce the Constructing Auxiliary Time Series (CATS) approach. CATS innovatively utilizes Auxiliary Time Series (ATS) to represent the inter-series relationship apart from the temporal relationship in the Original Time Series (OTS) X . The ATS is denoted as $A \in \mathbb{R}^{L \times N}$, where N is the total number of ATS. These ATS are generated by M ATS constructors $\{F_1, \dots, F_M\}$, with each constructor $F_m : \mathbb{R}^{L_I \times C} \rightarrow \mathbb{R}^{L_I \times n_m}$ responsible for creating n_m ATS, such that $\sum_{m=1}^M n_m = N$.

CATS Approach The CATS structure, as shown in Figure 3, while conducting the prediction of the original series, constructs ATS capable of representing inter-series relationships and incorporate the ATS predicting results into the OTS prediction to obtain the model output. In the absence of any ATS constructor, the output of CATS is identical to the result obtained by directly using a time series predictor. This predictor can be a univariate forecasting model or a multivariate forecasting model with neural network architecture. The

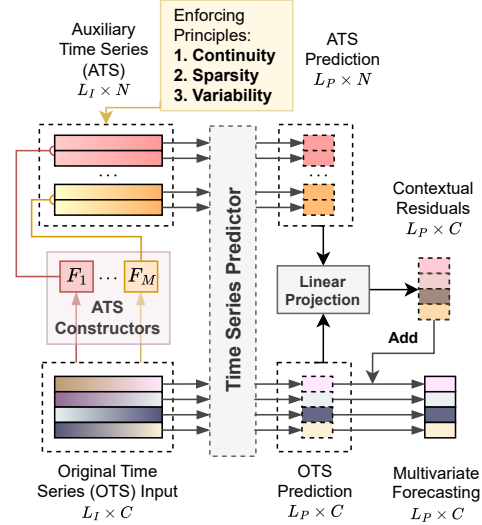


Figure 3. Overall Architecture of the CATS Approach

time series predictor is denoted as $\Phi_k : \mathbb{R}^{L_I \times k} \rightarrow \mathbb{R}^{L_P \times k}$, which is capable of mapping a specified k number of time series inputs from input to forecasting horizon. The prediction process of the model without ATS is expressed as $\hat{X}_P = \Phi_C(X_I)$. Let $[\dots]$ denotes concatenation along the series channel dimension. With ATS A , the predicting process for the combined set of $N + C$ time series becomes $[\hat{A}_P, \hat{X}_P] = \Phi_{N+C}([A_I, X_I])$, where

$$A_I = [F_1(X_I), F_2(X_I), \dots, F_M(X_I)] \in \mathbb{R}^{L_P \times N}.$$

The original \hat{X}_P part of the prediction¹ is retained as an OTS shortcut, encompassing most of the intra-series temporal relationship. For the remaining \hat{A}_P , concatenated with \hat{X}_P , we then project the $N + C$ result channels at each timestep into the C -dimensional space of the OTS, yielding the \tilde{X}_P that primarily captures the multivariate relationship. The process can be expressed as: $\tilde{X}_P^{(t),i} = \sum_{j=1}^{N+C} P_{ij} \cdot [\hat{A}_P^{(t)}, \hat{X}_P^{(t)}]_j$, where \tilde{X}_P denotes the integrated prediction, and P denotes the linear mapping matrix.

Finally, we can directly add the inter-series relationship component as the residual part to merge the prediction results as $\hat{X}_P^* = \hat{X}_P + \tilde{X}_P$, where \hat{X}_P^* represents the final forecasting after correcting with multivariate information.

3.1. Three Key Principles of ATS

This section discusses three critical principles—continuity, sparsity, and variability—that substantially boost model performance. These principles are critical for ATS to effectively extract useful information and accurately represent

¹For distinction purposes, we use the term *prediction* to denote the computation results of ATS and OTS over L_P , and the term *forecasting* for the combined final output of the model.

inter-series dependencies for correct pattern fitting.

3.1.1. CONTINUITY

Continuity is an important and inherent characteristic for most real-world time series datasets. We use a continuity loss term $\mathcal{L}_{\text{cont}}$ to enforce this principle of continuity in ATS:

$$\mathcal{L}_{\text{cont}} = \frac{\beta_{\text{cont}}}{L_I N} \sum_{t=2}^{L_I} \sum_{n=1}^N \left(\frac{A^{(t),n} - A^{(t-1),n}}{\sigma_n} \right)^2$$

where β_{cont} is a weighting factor that adjusts the influence of the continuity loss in the overall loss function. σ_n is standard deviation of the ATS for channel n .

By applying continuity loss, ATS will smooth out temporal details and noise, focusing on overall trends that can be described by inter-series dependencies, leaving the remaining intra-series details to be better modeled by established methods on the OTS. This clear division of modeling focus using ATS and OTS enhances the reliability and reduces the complexity of forecasting. We further investigate this from two theoretical perspectives. Detailed explanation of this part can be found in Appendix B.1.

Spectral Density and Filtering The introduction of continuity loss in ATS can be regarded as applying a low-pass filter. This filter effectively diminishes the high-frequency components in the ATS, making it smoother and less sensitive to noise. This can be expressed as a modification of the spectral density $S_X(f)$ of X , where $S_A(f) = S_X(f) \cdot H(f)$, with $H(f)$ being the low-pass filter. Consequently, the ATS focuses more on the overall trends rather than short-term fluctuations, providing a clearer representation of inter-series relationships.

Quadratic Variation and Denoising From the perspective of quadratic variation, continuity in the CATS model aids in reducing the ATS volatility. For a Brownian motion-driven process $X(t)$, the quadratic variation is significant. However, for ATS $A(t)$ with its quadratic variation close to zero, it will show more properties like a continuous differentiable function. This reduction in quadratic variation indicates that ATS with continuity becomes smoother and less prone to fluctuations like white noise, thereby enhancing the ability to capture and represent more long-term trends in the OTS.

Therefore, with continuity loss, the ATS prediction component \tilde{X}_P will primarily extract inter-series trends, allowing the OTS prediction component \hat{X}_P to focus on the more stable intra-series autocorrelation. This aligns perfectly with the structure and objectives of CATS.

3.1.2. SPARSITY

Channel Sparsity In CATS, ATS are tasked with representing inter-series dependencies. Therefore, when there are

more ATS channels, they tend to capture more inter-series information to influence the final forecasting. For many datasets where inter-series dependencies are weak, forcibly seeking them can lead to significant overfitting. Ideally, the number of available ATS should adaptively decrease when dealing with datasets that have weaker multivariate relationships. By activating only the most crucial ATS channels, model stability and performance would significantly improve. It also reduces the tuning cost for the hyperparameter of the number of ATS series. We refer to this as the principle of channel sparsity.

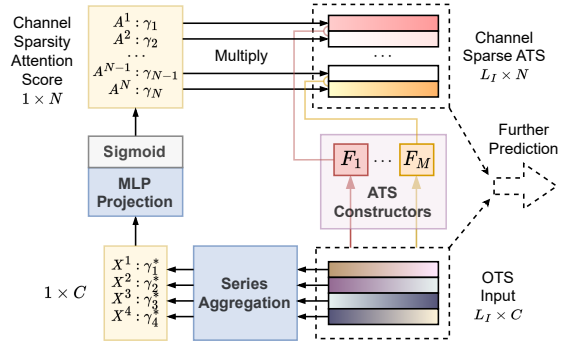


Figure 4. Channel Attention Score Calculation of Channel Sparsity

A mechanism is designed to allow the model to dynamically activate a varying number of ATS based on the strength of inter-series relationships, as shown in Figure 4. Similar to the channel attention mechanism commonly used in computer vision (Wang et al., 2017; Hu et al., 2018), this method aggregates the input OTS channels and conducts upscaling projection to obtain attention scores for each ATS channel. Ideally, the channel sparsity attention scores should be mostly zeros. However, to prevent the ATS from being insufficiently trained due to gradient problems, we use soft attention scores instead of hard channel dropping here.

For the OTS input $X_I \in \mathbb{R}^{L_I \times C}$, we first aggregate each series i through a linear layer to obtain the corresponding scalar γ_i^* , which can be expressed as $\gamma_i^* = \mathbf{w}^\top X^i + b$, where $\mathbf{w} \in \mathbb{R}^{L_I}$ and $b \in \mathbb{R}$ are the weight and bias of the linear layer. Then, we combine all γ_i^* into a vector and pass it through an upscaling MLP with activation to obtain the attention score γ_n for each ATS, which can be described as:

$$\gamma = \text{Sigmoid}(W_2 \cdot \text{GELU}(W_1 \gamma^* + \mathbf{b}_1) + \mathbf{b}_2)$$

where $\gamma^* = [\gamma_1^*, \gamma_2^*, \dots, \gamma_C^*]^\top$, $W_1 \in \mathbb{R}^{U \times C}$ and $W_2 \in \mathbb{R}^{N \times U}$ are the weights of the MLP, $\mathbf{b}_1 \in \mathbb{R}^U$ and $\mathbf{b}_2 \in \mathbb{R}^N$ are the biases of the MLP, and U is the dimension of the hidden layer. The applying of γ on A_I can be represented as: $A'_I = A_I \odot \gamma$, where A'_I is the adjusted ATS after applying the attention scores γ , \odot denotes element-wise multiplication. γ are used to suppress those unimportant

ATS channels, thus allowing the strength of the inter-series relationships represented by ATS to dynamically self-adjust.

Temporal Sparsity Previous MTSF research has shown that altering the length L_I significantly impacts model performance, leading most models to conduct hyper-parameter tuning of L_I (Wu et al., 2021; Zhou et al., 2022; Zeng et al., 2023; Nie et al., 2022; Lu et al., 2023). Choosing a too short L_I may fail to learn the correct dependencies, while a too long L_I can result in overfitting. Clearly, a fixed L_I for all the series is not the optimal choice. We need a mechanism to adaptively cutoff the time series input of the predictor. In this scenario, each channel can discard different lengths of long-term parts that are unnecessary for its prediction. Hence, the predictor input will include time series of varying lengths. We refer to this principle as temporal sparsity.

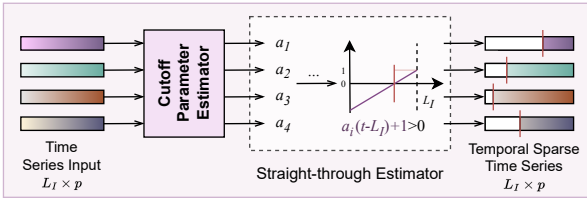


Figure 5. Adaptive Temporal Cutoff of Temporal Sparsity

An adaptive temporal cutoff method is designed to determine the required cutoff length for each series, as shown in Figure 5. Let the input series at this stage be $Q_I \in \mathbb{Q}^{L_I \times p}$ with p channels. We use a parameter a_i to determine the cutoff length for each series Q^i . For every Q^i , due to potential differences in properties, we assign independent linear layers to calculate their $a_i = \mathbf{W}^i Q_I^i + \mathbf{b}_i$, where $\mathbf{W} \in \mathbb{R}^{L_I \times p}$ and $\mathbf{b} \in \mathbb{R}^p$ are weights and biases. Then, we construct a linear function $h_i(t)$ as our hard cutoff function, where t is each timestep. We calculate $h_i(t) = a_i(t - L_I) + 1$, and determine whether $h_i(t) > 0$ is true for each step t to obtain the cutoff result $Q^{(t),i} = Q^{(t),i} \cdot \mathbf{1}_{\{h_i(t) > 0\}}$, where $\mathbf{1}_{\{\cdot\}}$ is the indicator function. If the inequality is not true, we set the value at t to 0, thus achieving the purpose of cutting off the earlier part of the series. However, this indicator function is not differentiable and may disrupt the learning. Therefore, we use a straight-through estimator, copying the gradient of $Q^{(t),i}$ to $Q^{(t),i}$ to bypass this non-differentiable part. Then, $Q^{(t),i}$ becomes:

$$Q_i^{(t)} = Q_i^{(t)} \cdot (h_i(t) - \text{sg}(h_i(t) + \mathbf{1}_{\{h_i(t) > 0\}}))$$

where $\text{sg}(\cdot)$ denotes the stop-gradient operation. Through this method, we obtain a time series with temporal sparsity after dynamic truncation. In the implementation, we apply the temporal sparsity module on both the ATS and OTS.

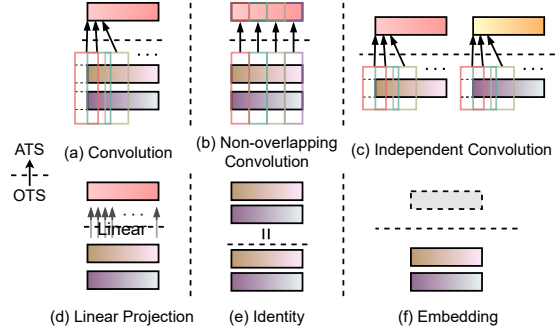


Figure 6. Different Types of ATS Constructors

3.1.3. VARIABILITY

Variability represents the diversity of inter-series dependencies that ATS can capture, reflecting how effectively OTS information is combined in varied ATS from multiple perspectives. This approach helps to prevent the forecasting from being controlled by a specific type of ATS, allowing the model to adapt to diverse MTSF datasets with different characteristics of dependency. CATS achieves this through a variety of ATS constructors with differing structures.

3.2. ATS Constructors

We develop a series of ATS constructors F_m as shown in Figure 3.2. With the benefits of CATS, we can simultaneously use multiple different structures as feature extractors. This allows us to surpass the constraints of previous MTSF models, which often restrict themselves to specific types of temporal processing methods. Note that we use GELU activation after each F_m to add non-linearity. The settings of ATS constructors used in our experiments are detailed in Appendix C.1 and Table 6.

Convolution is a prevalent temporal feature extractor that is capable of learning the contribution of local patterns to forecasting. The impact of varying kernel sizes in convolution is well-documented. (Lai et al., 2018; Borovykh et al., 2017; van den Oord et al., 2016; Li et al., 2019; Lu et al., 2023). CATS employs convolution layers with different kernel sizes as ATS constructors to accommodate different scenarios. The m th constructor utilizes 1D convolution $\text{Conv1d}_{[C \rightarrow n_m]}(\cdot, K, D, S, G)$, defined by kernel size K , padding D , stride S , channel groups G , and the n_m output channels mapped from C OTS. The constructor is given by: $F_m^{[\text{Conv}]}(X_I) = \text{Conv1d}_{[C \rightarrow n_m]}(X_I^\top, K, \lfloor \frac{K-1}{2} \rfloor, 1, 1)^\top$.

Non-overlapping Convolution, similar to patching, temporal aggregation, or hierarchical grouping, uses a convolution layer with kernel size equal to stride, which is widely applied in computer vision and time series (Dosovitskiy et al., 2021; Liu et al., 2021; Nie et al., 2022). Since we should keep the output length as L_I , we need some extra

padding $E = (K - (L_I \bmod K)) \bmod K$ and for each input-to-output patch, do K times of Conv1d calculation: $F_m^{\text{[NOConv]}}(X_I) = \text{Conv1d}_{[C \rightarrow n_m]}(X_I^\top, K, \lfloor \frac{E}{2} \rfloor, K, 1)^\top$.

Independent Convolution performs 1D convolution on each series separately. The ability of independent convolution to capture effective univariate features has been widely validated in previous research (Lai et al., 2018; Borovykh et al., 2017). By extracting local features independently for each series, it enhances ATS’s capability to recognize important series and avoids timestep mixing errors. The number of output channels could be $n_m = v \cdot C$, where $v \in \mathbb{Z}^+$. The constructor can be expressed as: $F_m^{\text{[IConv]}}(X_I) = \text{Conv1d}_{[C \rightarrow v \cdot C]}(X_I^\top, K, \lfloor \frac{K-1}{2} \rfloor, 1, C)^\top$.

Linear Projection This fundamental feature extractor linearly maps OTS across channels to form latent auxiliary series. Frequently used in MTSF models like Transformers and MLP-Mixers for input processing (Zhou et al., 2021; Wu et al., 2021; Zhang & Yan, 2023), linear projection offers a straightforward dimensional transformation. However, it can mix unrelated series, a risk CATS mitigates by combining various ATS constructors and retaining an OTS shortcut. This constructor is expressed as: $F_m^{\text{[Lin]}}(X_I) = \text{Conv1d}_{[C \rightarrow n_m]}(X_I^\top, 1, 0, 0, 1)^\top$

Identity Proven effective in §1.1, this method retains the input series’ original information, facilitating efficient learning of fundamental inter-series relationships like mapping and shifting. The constructor is simply: $F_m^{\text{[Id]}}(X_I) = X_I$.

Embedding involves a trainable matrix unrelated to OTS values but linked to timesteps. Similar to positional embeddings in Transformers, CATS adds embedding channels with time series properties, aiding in understanding temporal connections. The constructor, with a learnable matrix $\mathcal{W}^{\text{[Emb]}} \in \mathbb{R}^{n_m \times C}$, is: $F_m^{\text{[Emb]}}(X_I) = \mathcal{W}^{\text{[Emb]}}$.

3.3. Time Series Predictor

The enough inductive bias provided by CATS allows us to choose a simple main predictor Φ_{N+C} , whose primary task shifts to mapping the effective information from the input domain to the correct positions in the forecasting horizon. Thus, in the basic implementation, we simply use a two-layer MLP (2L) as the main predictor. Other structures, such as previous MTSF models (e.g., DLinear, Autoformer), independent linear layers (IndLin), and even the simplest average pooling (Mean), are also used in our ablation studies §4.1. For details on the structure of the predictors, see §B.2.

4. Experiments and Results

Comprehensive experiments were conducted on nine commonly-used MTSF datasets (details in Appendix A), including ETT (Zhou et al., 2021), Traffic, Electricity,

Weather, Exchange Rate (Lai et al., 2018), and Multi (Lu et al., 2023). We compared CATS against baseline models from six recent MTSF studies: ARM (Lu et al., 2023), PatchTST (Nie et al., 2022), DLinear (Zeng et al., 2023), FedFormer (Zhou et al., 2022), Autoformer (Wu et al., 2021), and Informer (Zhou et al., 2021). We use the same experiment environment as these models for fair comparison. In CATS, a structurally simple two-layer MLP (2L) was employed as the time series predictor to demonstrate CATS’s capability of empowering univariate models to effectively learn inter-series relationships. We use a total of 8 ATS constructors, detailed in Table 6. We trained CATS with a combination of Mean Squared Error (MSE) and continuity loss, using the Adam optimizer (Kingma & Ba, 2015). Also, we applied common training strategies from recent studies, including last-value demeaning and random dropping (Kim et al., 2022; Zeng et al., 2023; Lu et al., 2023). To identify the enhancement specific from CATS, these strategies were also applied across all baseline models in subsequent ablation studies (§4.1). Models from Informer to PatchTST required tuning of the input length L_I , selecting from $L_I \in \{96, 192, 336, 720\}$ for optimal results. However, CATS’s temporal sparsity module enables dynamic input cutoff for each channel, allowing a fixed $L_I = 720$. In the main text, the performance metrics used included averaged MSE and calculated average MSE percentage compared to a pivotal model on the test set. For original MSE and Mean Absolute Error (MAE) data, please refer to the Appendix D. Details on hyper-parameter settings and implementations can be found in Appendix C. Some visualization examples of ATS and OTS results can be found in Figure 7.

Main MTSF Experiment Results Table 1 highlights the superior performance of CATS across widely-used real-world datasets, outperforming existing MTSF models in average MSE and achieving a average ranking close to the first place. In 28 out of 36 sub-experiments for different L_P , CATS consistently delivered best outcomes (see Table 7). This reflects the significant enhancement brought by constructed ATS, thereby empowering the a simple univariate 2-layer MLP with temporal-contextual modeling capacity.

Extended MTSF Experiment Results In §1.1, we showed a shifting problem, which is introduced by ARM (Lu et al., 2023) to create the Multi dataset in our benchmarks to test models in strong multivariate relationship scenarios, where CATS demonstrated superior performance. To further assess CATS in more complex conditions with a greater number of series than 8 in Multi, we created the MultiX datasets. These datasets derive each series from a master AR(1) series, with each subsequent series lagging the previous by a set stride, adding and accumulating random noise in each shifting to challenge the model’s ability to learn generative dependencies rather than just relying on the first series. Eventually,

Table 1. Summary of MTSF results with forecasting horizons $L_P \in \{96, 192, 336, 720\}$. See Table 7 for original results. Averages of MSE results (in parentheses) for each model on each dataset and MSE percentages (above parentheses) relative to DLinear are provided. The best and second best results are in bold and underlined, respectively. Average percentages (Avg%) across all datasets and average rankings (AvgRank) of each model, along with the count of first-place rankings (#Win), are also included.

Models	CATS (2L)	ARM	PatchTST	DLinear	FedFormer	Autoformer	Informer
Electricity	89.6% (0.149)	<u>90.2%</u> (0.150)	95.6% (0.159)	100.0% (0.166)	128.4% (0.214)	136.5% (0.227)	186.9% (0.311)
ETTm1	96.5% (0.345)	<u>97.3%</u> (0.348)	98.8% (0.353)	100.0% (0.357)	107.1% (0.382)	144.3% (0.515)	244.3% (0.872)
ETTm2	91.0% (0.243)	<u>93.8%</u> (0.251)	95.9% (0.256)	100.0% (0.267)	113.9% (0.305)	121.3% (0.324)	527.6% (1.410)
ETTh1	96.6% (0.408)	<u>96.2%</u> (0.407)	97.7% (0.413)	100.0% (0.423)	101.2% (0.428)	111.9% (0.473)	244.2% (1.033)
ETTh2	72.8% (0.314)	<u>76.4%</u> (0.330)	76.7% (0.331)	100.0% (0.431)	89.9% (0.388)	97.9% (0.422)	765.9% (3.303)
Weather	85.3% (0.210)	<u>87.5%</u> (0.215)	91.7% (0.226)	100.0% (0.246)	125.5% (0.309)	137.3% (0.338)	257.6% (0.634)
Traffic	87.3% (0.379)	<u>88.6%</u> (0.384)	90.1% (0.391)	100.0% (0.434)	140.5% (0.610)	144.7% (0.628)	176.1% (0.764)
Exchange	84.7% (0.251)	<u>81.5%</u> (0.242)	126.4% (0.375)	100.0% (0.297)	174.9% (0.519)	206.8% (0.613)	522.9% (1.550)
Multi	70.9% (0.168)	<u>77.2%</u> (0.177)	136.5% (0.313)	100.0% (0.230)	132.2% (0.304)	195.5% (0.449)	163.8% (0.376)
Avg%	86.1%	<u>87.6%</u>	101.0%	100.0%	123.7%	144.0%	343.3%
AvgRank	1.25	<u>1.75</u>	3.47	3.83	5.11	6.28	7.39
#Win	28	<u>10</u>	1	0	0	0	0

Table 2. Summary of extended MTSF results on datasets with strong inter-series relationship. See Table 8 for original results. The method of displaying summary data is the same as in Table 1.

Models	CATS (2L)	ARM	PatchTST	DLinear	FedFormer	Autoformer	Informer
Multi20	67.0% (0.017)	<u>74.0%</u> (0.019)	109.7% (0.027)	100.0% (0.025)	230.7% (0.058)	230.3% (0.058)	338.3% (0.085)
Multi50	73.6% (0.018)	<u>82.7%</u> (0.021)	112.3% (0.028)	100.0% (0.025)	241.3% (0.060)	291.9% (0.072)	417.6% (0.104)
Multi100	71.7% (0.018)	<u>80.7%</u> (0.020)	111.4% (0.028)	100.0% (0.025)	232.6% (0.058)	475.1% (0.119)	445.8% (0.112)
Multi200	64.1% (0.017)	<u>89.4%</u> (0.023)	106.2% (0.027)	100.0% (0.026)	253.4% (0.065)	279.8% (0.072)	317.2% (0.082)
Avg%	69.1%	<u>81.7%</u>	109.9%	100.0%	239.5%	319.3%	379.7%
AvgRank	1.50	<u>1.94</u>	4.06	2.81	6.81	7.06	7.06
#Win	12	<u>1</u>	0	3	0	0	0

the final series is noised offset from the first by a total of S steps. We set $S = L_I = 720$. If the number of extracted series, X , is 100, the dataset is named Multi100, and so forth. More details about this dataset are in Appendix A.

Table 2 shows CATS’s exceptional performance in MultiX scenarios. CATS significantly outperforms previous models in average MSE and achieves the best results in 12 out of 16 sub-experiments. The original results in Table 8 reveals that CATS markedly surpasses previous models when $L_P \in \{96, 192, 336\}$, where true inter-series relationships are more prevalent. It’s noteworthy that when forecasting horizon L_P extends to 720, CATS’s performance aligns more closely with traditional models. This pattern can be attributed to the reduced presence of actual inter-series dependencies in the input series for longer L_P values. In essence, as the forecasting horizon expands, the influence of true inter-series relationships diminishes, leading to a scenario resembling a univariate AR(1) prediction with noise.

In such cases, CATS’s channel sparsity feature becomes more prominent, effectively reducing the ATS’s influence and reverting the model to a simpler form of a univariate MLP. This behavior demonstrates CATS’s adaptability in handling varying strengths of multivariate relationships.

4.1. Ablation Studies

In the ablation studies, we apply CATS to basic time series predictors and previous MTSF models to demonstrate the enhancement attributed to the CATS structure. We also show the effects of the three key principles of ATS. For the experiments, we select two datasets, Multi and ETTh2, which respectively represent scenarios with strong and weak inter-series dependencies. To eliminate the impact of training strategies, including last-value demeaning and random dropping, we implement these strategies across all baseline models during training. We fix the input length $L_I = 720$ and only alter the elements of CATS components described in Figure 3, while keeping all other settings constant.

Time Series Predictors + CATS In Table 3, we apply the CATS structure to a univariate model (DLinear), a multivariate model (Autoformer), and three basic univariate predictors (2L, IndLin, Mean). IndLin represents the use of independent linear layers for each ATS/OTS prediction. Mean fills the corresponding L_P region for each ATS/OTS with its mean value of the input.

The integration of CATS significantly enhances the performance of each baseline. Examining the original results in Table 9, we find that CATS provides significant and stable performance enhancements in scenarios with strong multivariate relationships and effectively suppresses overfitting when these relationships are weaker, ensuring better results than the baselines. These enhancements are independent of the predictor’s structure. Even when the predictor is merely performing an average pooling (Mean), CATS is still able to transfer the inter-series relationships into the OTS output, surpassing the performance of most baselines. Note that IndLin performs the best in the sub-experiments with very strong inter-series dependencies, as shown in Table 9, which aligns with the example in §1.1. This highlights the powerful and flexible foundational fitting ability provided by the 2D attention-like structure for multivariate modeling.

Three ATS Principles Table 4 investigates the influence of key principles on performance. It shows that the absence of any principles significantly diminishes performance.

Continuity allows the ATS to focus more on inter-series trend effects, enabling the OTS part to better model the stabler autocorrelation after removing the inter-series long-term trend. This enhancement is particularly notable in ETTh2, characterized by many long-term trend changes.

Regarding sparsity, removing both sparsity modules dras-

Table 3. Summary of results for using CATS with time series predictors. See Table 9 for original results. We compared the average MSE before and after using CATS and calculated the percentage based on the averages without CATS. Better results are highlighted in bold.

Models	2L	2L +CATS	DLinear	DLinear +CATS	Autoformer	Autoformer +CATS	IndLin	IndLin +CATS	Mean	Mean +CATS
Multi	100.0% (0.360)	45.2% (0.163)	100.0% (0.286)	63.2% (0.181)	100.0% (0.595)	36.0% (0.214)	100.0% (0.291)	57.7% (0.168)	100.0% (0.654)	37.9% (0.248)
ETTh2	100.0% (0.348)	90.3% (0.314)	100.0% (0.341)	98.1% (0.335)	100.0% (0.390)	89.8% (0.351)	100.0% (0.340)	98.8% (0.336)	100.0% (0.408)	92.6% (0.378)

Table 4. Summary of the ablation studies of the three ATS principles and OTS shortcut. See Table 10 for original results. We calculated the average MSE and percentages based on the full CATS model to show the impact of these components on the model performance.

Models	CATS (2L)	w/o Continuity	w/o Sparsity (Channel)	w/o Sparsity (Temporal)	w/o Sparsity (Both)	w/o Variability (Pure Linear)	w/o Variability (Pure Conv)	w/o OTS Shortcut
Multi	100.0% (0.163)	141.9% (0.231)	156.7% (0.255)	126.4% (0.206)	158.4% (0.258)	146.1% (0.238)	122.1% (0.199)	128.3% (0.209)
ETTh2	100.0% (0.314)	103.5% (0.325)	103.2% (0.324)	104.1% (0.327)	105.3% (0.330)	104.1% (0.327)	104.2% (0.327)	109.6% (0.344)

tically reduces performance. In the Multi dataset, where we aim to model numerous inter-series relationships using a sufficient number of ATS series, selecting the important series is vital to prevent overfitting. In ETTh2, characterized by weaker multivariate effects, using channel sparsity to manage ATS strength significantly enhances outcomes. Also, adjusting L_I has been shown to affect ETTh2’s results markedly (Nie et al., 2022; Zeng et al., 2023). Implementing temporal sparsity for dynamic lookback further improves performance.

Variability influences the scope of inter-series dependencies captured by ATS. We tested this by altering ATS constructors: first, all constructors were changed to linear projections (Pure Linear), leading to reduced performance on both datasets. Next, using solely 1D convolutions (Pure Conv) also fell short compared to a mix of constructors, but slightly outperformed Pure Linear on the Multi dataset, highlighting the importance of local and series-independent feature processing for stronger inter-series relationship representation.

We assessed the effect of the OTS shortcut on performance. This feature, alongside sparsity, guarantees that CATS’s results are at least as good as the base model. In ETTh2, characterized by weaker inter-series and stronger intra-series dependencies, removing the OTS shortcut led to significant performance drops due to the loss of series-wise independence, leading to improper mixing of series information in ATS-to-OTS projections. This highlights how the integration of various CATS structural components adaptively enhances performance.

Computational Costs As illustrated in Table 5, compared to Transformer-based models like ARM, Autoformer, Informer, and PatchTST, CATS significantly reduces both computational complexity and parameter size. When compared with simple univariate models such as DLinear, CATS effectively models varying strengths of inter-series dependencies with an acceptable incremental computational cost. Consequently, CATS can be characterized as a lightweight, low-complexity, and easily transferable structure for MTSF.

Table 5. Comparison of computational costs. This comparison utilizes the data format of ETTh2 to construct model inputs. L_I is set to 720, and the other hyper-parameters for every model are set according to their default configurations.

Models	CATS (2L)		ARM		Autoformer	
	FLOPs	Params	FLOPs	Params	FLOPs	Params
$L_P = 96$	382M	2.47M	426M	7.89M	10.9G	15.5M
$L_P = 192$	422M	2.74M	515M	10.4M	11.6G	15.5M
$L_P = 336$	483M	3.16M	664M	14.9M	12.7G	15.5M
$L_P = 720$	645M	4.26M	1.15G	30.6M	15.5G	15.5M

Models	Informer		PatchTST		DLinear	
	FLOPs	Params	FLOPs	Params	FLOPs	Params
$L_P = 96$	9.41G	11.3M	5.26G	4.87M	3.06M	138K
$L_P = 192$	10.1G	11.3M	5.31G	7.08M	6.10M	277K
$L_P = 336$	11.2G	11.3M	5.38G	10.4M	10.7M	485K
$L_P = 720$	14.0G	11.3M	5.58G	19.2M	22.8M	1.04M

5. Conclusion, Future Works, and Limitation

In this study, we address the counter-intuition observed in MTSF where univariate models often outperform multivariate ones, despite the latter’s ability to capture inter-series relationships. Our approach, Constructing Auxiliary Time Series (CATS), enhances forecasting by generating ATS from OTS to represent inter-series relationships. CATS’s efficacy is anchored in three key ATS principles — continuity, sparsity, and variability — along with the maintenance of the OTS shortcut. Our experiments reveal that CATS, even when paired with very simple predictor structures, significantly outperforms existing models in both strong and weak multivariate relationship scenarios. Furthermore, CATS offers a significant reduction in computational complexity and parameter size compared to other multivariate models, marking it as an easy-to-implement solution for MTSF.

For future works, CATS has the potential to be expanded into a general sequential modeling solution. With a wide range of ATS constructing methods and an increase in parameter size (such as using scalable Mixture of Experts for ATS construction, prediction, and projection), ATS can integrate very complex sequential relationships and perform efficient 2D attention-like operations. This gives it the potential to be transferred to fields like NLP and audio. CATS also

has certain limitations: when constructing a fixed number of ATS, although it can address weak multivariate relationships through sparsity, if such relationships are too complex and require more ATS than the set number, the current CATS cannot expand automatically during training.

References

- Borovykh, A., Bohte, S., and Oosterlee, C. W. Conditional time series forecasting with convolutional neural networks. *ArXiv preprint*, abs/1703.04691, 2017. URL <https://arxiv.org/abs/1703.04691>.
- Box, G. E., Jenkins, G. M., and MacGregor, J. F. Some recent advances in forecasting and control. *Journal of the Royal Statistical Society: Series C (Applied Statistics)*, 23(2):158–179, 1974.
- Dosovitskiy, A., Beyer, L., Kolesnikov, A., Weissenborn, D., Zhai, X., Unterthiner, T., Dehghani, M., Minderer, M., Heigold, G., Gelly, S., Uszkoreit, J., and Houshy, N. An image is worth 16x16 words: Transformers for image recognition at scale. In *International Conference on Learning Representations*, 2021. URL <https://openreview.net/forum?id=YicbFdNTTy>.
- Hochreiter, S. and Schmidhuber, J. Long short-term memory. *Neural computation*, 9(8):1735–1780, 1997.
- Holt, C. C. Forecasting seasonals and trends by exponentially weighted moving averages. *International journal of forecasting*, 20(1):5–10, 2004.
- Hu, J., Shen, L., and Sun, G. Squeeze-and-excitation networks. In *Proceedings of the IEEE Conference on Computer Vision and Pattern Recognition (CVPR)*, June 2018.
- Kaasra, I. and Boyd, M. Designing a neural network for forecasting financial and economic time series. *Neurocomputing*, 10(3):215–236, 1996.
- Kim, T., Kim, J., Tae, Y., Park, C., Choi, J., and Choo, J. Reversible instance normalization for accurate time-series forecasting against distribution shift. In *The Tenth International Conference on Learning Representations, ICLR 2022, Virtual Event, April 25-29, 2022*. OpenReview.net, 2022. URL <https://openreview.net/forum?id=cGDAkQo1C0p>.
- Kingma, D. and Ba, J. Adam: A method for stochastic optimization. In *International Conference on Learning Representations (ICLR)*, San Diego, CA, USA, 2015.
- Lai, G., Chang, W., Yang, Y., and Liu, H. Modeling long- and short-term temporal patterns with deep neural networks. In Collins-Thompson, K., Mei, Q., Davison, B. D., Liu, Y., and Yilmaz, E. (eds.), *The 41st International ACM SIGIR Conference on Research & Development in Information Retrieval, SIGIR 2018, Ann Arbor, MI, USA, July 08-12, 2018*, pp. 95–104. ACM, 2018. doi: 10.1145/3209978.3210006. URL <https://doi.org/10.1145/3209978.3210006>.
- Li, S., Jin, X., Xuan, Y., Zhou, X., Chen, W., Wang, Y., and Yan, X. Enhancing the locality and breaking the memory bottleneck of transformer on time series forecasting. In Wallach, H. M., Larochelle, H., Beygelzimer, A., d’Alché-Buc, F., Fox, E. B., and Garnett, R. (eds.), *Advances in Neural Information Processing Systems 32: Annual Conference on Neural Information Processing Systems 2019, NeurIPS 2019, December 8-14, 2019, Vancouver, BC, Canada*, pp. 5244–5254, 2019. URL <https://proceedings.neurips.cc/paper/2019/hash/6775a0635c302542da2c32aa19d86be0-Abstract.html>.
- Liu, Y., Hu, T., Zhang, H., Wu, H., Wang, S., Ma, L., and Long, M. itransformer: Inverted transformers are effective for time series forecasting, 2023.
- Liu, Z., Lin, Y., Cao, Y., Hu, H., Wei, Y., Zhang, Z., Lin, S., and Guo, B. Swin transformer: Hierarchical vision transformer using shifted windows. In *Proceedings of the IEEE/CVF international conference on computer vision*, pp. 10012–10022, 2021.
- Lu, J., Han, X., and Yang, S. Arm: Refining multivariate forecasting with adaptive temporal-contextual learning, 2023.
- Ma, S., Sun, Y., and Yang, S. Using internet search data to forecast covid-19 trends: A systematic review. *Analytics*, 1(2):210–227, 2022. ISSN 2813-2203. doi: 10.3390/analytics1020014. URL <https://www.mdpi.com/2813-2203/1/2/14>.
- Nie, Y., Nguyen, N. H., Sinthong, P., and Kalagnanam, J. A time series is worth 64 words: Long-term forecasting with transformers. In *The Eleventh International Conference on Learning Representations*, 2022.
- Nihan, N. L. and Holmesland, K. O. Use of the box and jenkins time series technique in traffic forecasting. *Transportation*, 9(2):125–143, 1980.
- Qin, Y., Song, D., Chen, H., Cheng, W., Jiang, G., and Cottrell, G. W. A dual-stage attention-based recurrent neural network for time series prediction. In Sierra, C. (ed.), *Proceedings of the Twenty-Sixth International Joint Conference on Artificial Intelligence, IJCAI 2017, Melbourne, Australia, August 19-25, 2017*, pp. 2627–2633. ijcai.org, 2017. doi: 10.24963/ijcai.2017/366. URL <https://doi.org/10.24963/ijcai.2017/366>.

- Rangapuram, S. S., Seeger, M. W., Gasthaus, J., Stella, L., Wang, Y., and Januschowski, T. Deep state space models for time series forecasting. In Bengio, S., Wallach, H. M., Larochelle, H., Grauman, K., Cesa-Bianchi, N., and Garnett, R. (eds.), *Advances in Neural Information Processing Systems 31: Annual Conference on Neural Information Processing Systems 2018, NeurIPS 2018, December 3-8, 2018, Montréal, Canada*, pp. 7796–7805, 2018. URL <https://proceedings.neurips.cc/paper/2018/hash/5cf68969fb67aa6082363a6d4e6468e2-Abstract.html>.
- Salinas, D., Flunkert, V., Gasthaus, J., and Januschowski, T. Deepar: Probabilistic forecasting with autoregressive recurrent networks. *International Journal of Forecasting*, 36(3):1181–1191, 2020.
- Sims, C. A. Macroeconomics and reality. *Econometrica*, 48(1):1–48, 1980. ISSN 00129682, 14680262. URL <http://www.jstor.org/stable/1912017>.
- Sun, Y. and Yang, S. Manifold-constrained gaussian process inference for time-varying parameters in dynamic systems. *Statistics and Computing*, 33(6):142, 2023.
- van den Oord, A., Dieleman, S., Zen, H., Simonyan, K., Vinyals, O., Graves, A., Kalchbrenner, N., Senior, A., and Kavukcuoglu, K. Wavenet: A generative model for raw audio. In *9th ISCA Speech Synthesis Workshop*, pp. 125–125, 2016.
- Wang, F., Jiang, M., Qian, C., Yang, S., Li, C., Zhang, H., Wang, X., and Tang, X. Residual attention network for image classification. In *Proceedings of the IEEE conference on computer vision and pattern recognition*, pp. 3156–3164, 2017.
- Wen, Q., Zhou, T., Zhang, C., Chen, W., Ma, Z., Yan, J., and Sun, L. Transformers in time series: A survey. *arXiv preprint arXiv:2202.07125*, 2022.
- Wen, R., Torkkola, K., Narayanaswamy, B., and Madeka, D. A multi-horizon quantile recurrent forecaster. *ArXiv preprint*, abs/1711.11053, 2017. URL <https://arxiv.org/abs/1711.11053>.
- Wu, H., Xu, J., Wang, J., and Long, M. Autoformer: Decomposition transformers with auto-correlation for long-term series forecasting. In Ranzato, M., Beygelzimer, A., Dauphin, Y. N., Liang, P., and Vaughan, J. W. (eds.), *Advances in Neural Information Processing Systems 34: Annual Conference on Neural Information Processing Systems 2021, NeurIPS 2021, December 6-14, 2021, virtual*, pp. 22419–22430, 2021. URL <https://proceedings.neurips.cc/paper/2021/hash/bcc0d400288793e8bdcd7c19a8ac0c2b-Abstract.html>.
- Zeng, A., Chen, M., Zhang, L., and Xu, Q. Are transformers effective for time series forecasting? In *Proceedings of the AAAI conference on artificial intelligence*, volume 37, pp. 11121–11128, 2023.
- Zhang, Y. and Yan, J. Crossformer: Transformer utilizing cross-dimension dependency for multivariate time series forecasting. In *The Eleventh International Conference on Learning Representations*, 2023.
- Zhou, H., Zhang, S., Peng, J., Zhang, S., Li, J., Xiong, H., and Zhang, W. Informer: Beyond efficient transformer for long sequence time-series forecasting. In *Thirty-Fifth AAAI Conference on Artificial Intelligence, AAAI 2021, Thirty-Third Conference on Innovative Applications of Artificial Intelligence, IAAI 2021, The Eleventh Symposium on Educational Advances in Artificial Intelligence, EAAI 2021, Virtual Event, February 2-9, 2021*, pp. 11106–11115. AAAI Press, 2021. URL <https://ojs.aaai.org/index.php/AAAI/article/view/17325>.
- Zhou, T., Ma, Z., Wen, Q., Wang, X., Sun, L., and Jin, R. Fedformer: Frequency enhanced decomposed transformer for long-term series forecasting. In Chaudhuri, K., Jegelka, S., Song, L., Szepesvári, C., Niu, G., and Sabato, S. (eds.), *International Conference on Machine Learning, ICML 2022, 17-23 July 2022, Baltimore, Maryland, USA*, volume 162 of *Proceedings of Machine Learning Research*, pp. 27268–27286. PMLR, 2022. URL <https://proceedings.mlr.press/v162/zhou22g.html>.

A. Datasets

We conduct our main MTSF experiments on 9 commonly used time series forecasting datasets, summarized as follows:

ETT Dataset² (Zhou et al., 2021), encompassing load and oil temperature data of electricity transformers, is recorded at 15-minute intervals from July 2016 to July 2018. It consists of four subsets: ETTm1, ETTm2, ETTh1, and ETTh2, representing two transformers (identified as 1 and 2) and two time resolutions (15 minutes and 1 hour). Each subset contains seven features related to oil and load of electricity transformers.

Electricity Dataset³, covering hourly electricity usage data of 321 consumers from 2012 to 2014, is frequently utilized in energy consumption forecasting and analysis.

Exchange Dataset⁴ (Lai et al., 2018), comprising daily exchange rates of eight countries from 1990 to 2016, offers insights into the global financial market dynamics.

Traffic Dataset⁵, sourced from freeway sensors in the San Francisco Bay area, provides hourly road occupancy data from 2015 to 2016, serving as a key resource for traffic flow studies.

Weather Dataset⁶ captures 21 weather variables, like temperature and humidity, recorded every 10 minutes throughout 2020, aiding in detailed meteorological studies.

Multi Dataset (Lu et al., 2023) is generated based on a master random walk series. The first series is the master series, and the second to fifth series are derived by shifting the first series backward by 96, 192, 336, and 720 steps, respectively. The last three series are combinations of the first five series.

MultiX Dataset is also generated based on a master random walk series. It comprises X series, where the first series is the master series, and each subsequent series is derived by shifting the previous series backward by $\frac{720}{X}$ steps. Before each shift, cumulative random noise is added to create a generative relationship with rich dependencies.

B. Additional Explanation of Model Structure

B.1. Continuity

Latent Separation of Inter-series Trend Effects As aforementioned, in most real-world datasets, the univariate contribution tends to dominate in forecasting. The intra-series relationship here, in other words, the autocorrelation function (ACF) of the time series, governs their shape details. Considering a local temporal signal $X(t)$, its ACF $R_X(\tau) = \mathbb{E}[(X(t) - \mu_X)(X(t + \tau) - \mu_X)]$ describes the correlation of the signal with itself at different lags τ , where μ_X is the mean of $X(t)$. Even if a series is entirely generated by several other series, we can still establish its own shape-defining ACF based on the ACF of these other series. Considering a set of multivariate signals $\{X_j(t)\}$, assuming $X_i(t)$ is completely generated by other local signals $\{X_j(t)\}_{j \neq i}$ which can be explained by local ACF $R_{X_j(t)}$, it can be represented as: $X_i(t) = g_i(\{R_{X_j(t)}\}_{j \neq i})$, where g_i is a generating function for local process i . The autocorrelation function $R_{X_i}(\tau)$ of $R_{X_j(t)}$ is then expressed as:

$$R_{X_i}(\tau) = \mathbb{E}[(g_i(\{R_{X_j(t)}\}_{j \neq i}) - \mu_{X_i})(g_i(\{R_{X_j(t+\tau)}\}_{j \neq i}) - \mu_{X_i})].$$

In this generative system, since that only term that may not come from the series itself is μ_{X_i} , if the trend in $X_i(t)$ is controlled, meaning μ_{X_i} is fixed, even if $X_i(t)$ is entirely generated by other series, its autocorrelation function $R_{X_i(t)}(\tau)$ will remain determinable in this system, which becomes non-local ACF $R_{X_i}(\tau)$. This actually means that the more μ_{X_i} we explain by using inter-series information (the intra-series effects of μ_{X_i} can equally be considered as inter-series effects without affecting our derivation), the more stable this system will be. Therefore, when we can explain more of the internal

²<https://github.com/zhouhaoyi/ETDataset>

³<https://archive.ics.uci.edu/ml/datasets/ElectricityLoadDiagrams20112014>

⁴<https://github.com/laiguokun/multivariate-time-series-data>

⁵<http://pems.dot.ca.gov/>

⁶<https://www.bgc-jena.mpg.de/wetter/>

trend changes of a series using information beyond the series, the resulting more stable autocorrelation function can both enhance the reliability of forecasting and greatly reduce the complexity required by the main predictor. Consequently, the OTS part of CATS essentially computes all $X(t) = \text{Predict}(R_{X(t)}(\tau), X(t-i))$, where $i \in 1, \dots, \tau$, using all stable ACFs. These ACFs, essentially latent functions within a neural network and not actual closed-form ACFs, enable the estimation of long-term detrend autocorrelations for all series by controlling the μ_X term. This approach separates the μ_X term latently in the CATS structure, thereby fixing the autocorrelation for each series and enabling the model to predict accurately through latent stable ACFs. In this scenario, the ATS’s ability to extract changes in trend becomes key to model performance.

Spectral Density We can use continuity loss to effectively enhance the ability of ATS to capture trends. Consider the spectral density of a local temporal signal $X(t)$, represented as

$$S_X(f) = \int_{-\infty}^{\infty} R_X(\tau) e^{-i2\pi f\tau} d\tau,$$

where f is the frequency. Let’s consider an ATS signal $A(t)$ generated based on $X(t)$. The continuity loss reduces the differences between adjacent points in ATS. Consequently, compared to $X(t)$, it imposes a penalty on the high-frequency components. This can be viewed as applying a low-pass filter $H(f)$ to ATS. Therefore, the autocorrelation function of ATS, $R_A(\tau) = R_X(\tau) * h(\tau)$, is influenced by this filtering, where $*$ denotes convolution and $h(\tau)$ is the inverse Fourier transform of $H(f)$. Here, the spectral density of $A(t)$ is

$$S_A(f) = \int_{-\infty}^{\infty} R_A(\tau) e^{-i2\pi f\tau} d\tau = S_X(f) \cdot H(f).$$

The $H(f)$ reduces the high-frequency components in $S_A(f)$, resulting in a lower amplitude of $A(t)$ at high frequencies compared to $X(t)$. This means that $A(t)$ contains fewer short-term fluctuations or noise. As a result, the constructed ATS is smoother, reducing sensitivity to noise and focusing more on long-term trends.

Quadratic Variation and Denoising The role of Continuity in the CATS model can be understood from the perspectives of Quadratic Variation and Denoising. This theoretical viewpoint reveals how continuity aids in removing white noise from the ATS system and smoothens ATS predictions.

For a random process driven by Brownian motion (B_t), the quadratic variation $[B]_a^b$ over the interval $[a, b]$ is equal to the length of the interval $b - a$. This indicates that the quadratic variation of Brownian motion is closely related to the volatility along its path. According to its fundamental theorem, the quadratic variation of any differentiable function over any interval is zero, reflecting the smooth nature of its trajectory. Consider an ATS $A(t)$, derived from an original time series $X(t)$. If $X(t)$ is driven by Brownian motion, then its quadratic variation over a certain interval is non-zero. However, by applying the Continuity principle, we aim to reduce the quadratic variation of $A(t)$. Let $A(t)$ be a continuous differentiable function, then its quadratic variation $[A]_a^b$ over the interval $[a, b]$ is zero, which implies:

$$[A]_a^b = \lim_{\|P\| \rightarrow 0} \sum_{i=1}^{n-1} (A(t_{i+1}) - A(t_i))^2 = 0$$

where P is a partition of the interval $[a, b]$. In the CATS approach, by introducing the Continuity principle, we aim to decrease the volatility of the ATS, endowing it with properties akin to a differentiable function. This effectively removes short-term fluctuations, or white noise, from the time series, enabling the ATS to capture more of the long-term trends present in the OTS.

B.2. Time Series Predictors

We introduce two predictor structures: the two-layer MLP (2L) and the independent linear layers (Ind) where weights are not shared between channels. The 2L predictor can be expressed as:

$$\Phi_{N+C}^{[2L]}([A_I, X_I]) = \mathcal{W}_2 \cdot \text{GELU}(\mathcal{W}_1 \cdot [A_I, X_I]^\top + \beta_1)^\top + \beta_2$$

where $\mathcal{W}_1, \mathcal{W}_2$ are the weight matrices for the two layers, and β_1, β_2 are the corresponding biases. The IndLin predictor can be expressed as:

$$\Phi_{N+C}^{[\text{IndLin}]}([A_I, X_I]^j) = \mathcal{W}^j \cdot [A_I, X_I]^j{}^\top + \beta^j$$

where \mathcal{W}^j is the weight vector and β^j is the bias for the linear layer of channel j . The Mean predictor can be expressed as:

$$\Phi_{N+C}^{[\text{Mean}]}([A_I, X_I]^j) = \frac{1}{L_I} \sum_{t=1}^{L_I} [A_I, X_I]^{(t),j} \cdot \mathbf{1}_{L_P}$$

where $\mathbf{1}_{L_P}$ is a ones vector with its length being L_P .

C. Implementation Details

C.1. Hyper-parameter Settings

We trained the CATS model using the Adam optimizer, employing a combined loss of Mean Squared Error (MSE) and a continuity loss term. The weight of continuity loss β_{cont} was set to 1. We used a learning rate of 0.00005, conducting training over 100 epochs with an early-stopping mechanism set at 30 steps. During these 100 epochs, a linear learning rate decay was applied. For all experiments, L_I was set to 720. The training utilized a single Nvidia RTX 4090 GPU with a batch size of 32. Input processing strategies included random dropping and last-value demeaning as described in the main text.

A total of eight ATS constructors were consistently used, **detailed in Table 6**. Datasets were classified into two categories: small datasets with $C < 16$ and large datasets with $C \geq 16$. The hyperparameter settings of ATS constructors for these two types of datasets are listed in Table 6. For the various 2-layer MLP structures in the text, the hidden layer dimension was set using a multiplier of q times the input dimension, where the MLP ratio is q . For small datasets, $q = 4$, and for large datasets, $q = 8$. The 2-layer predictor (2L) included a dropout layer in the hidden layer, with a dropout rate of 0.75 for small datasets and 0.5 for large datasets. Independent linear and mean predictors did not require hyperparameter settings. For other MTSF baseline models used, we followed the settings from their original papers.

For model selection, following previous MTSF research practices, each dataset was divided into 70% training, 10% validation, and 20% test sets. The best model was selected based on validation MSE loss, and MSE and MAE on the test set were calculated as reported results.

Table 6. Hyperparameter Settings of ATS Constructors

Constructor	Expression	Settings ($C < 16$)	Settings ($C \geq 16$)
Convolution (1)	$F_1^{[\text{Conv}]}(X_I) = \text{Conv1d}_{[C \rightarrow n_1]}(X_I^\top, K, \lfloor \frac{K-1}{2} \rfloor, 1, 1)^\top$	$K = 49, n_1 = 8$	$K = 49, n_1 = 32$
Convolution (2)	$F_2^{[\text{Conv}]}(X_I) = \text{Conv1d}_{[C \rightarrow n_2]}(X_I^\top, K, \lfloor \frac{K-1}{2} \rfloor, 1, 1)^\top$	$K = 193, n_2 = 8$	$K = 193, n_1 = 32$
Non-overlapping Convolution (1)	$F_3^{[\text{NOConv}]}(X_I) = \text{Conv1d}_{[C \rightarrow n_3]}(X_I^\top, K, \lfloor \frac{E}{2} \rfloor, K, 1)^\top$	$K = 12, n_3 = 8$	$K = 12, n_3 = 32$
Non-overlapping Convolution (2)	$F_4^{[\text{NOConv}]}(X_I) = \text{Conv1d}_{[C \rightarrow n_4]}(X_I^\top, K, \lfloor \frac{E}{2} \rfloor, K, 1)^\top$	$K = 24, n_4 = 8$	$K = 24, n_4 = 32$
Independent Convolution	$F_5^{[\text{IConv}]}(X_I) = \text{Conv1d}_{[C \rightarrow n_5]}(X_I^\top, K, \lfloor \frac{K-1}{2} \rfloor, 1, C)^\top$	$K = 49, n_5 = 1 \cdot C$	$K = 49, n_5 = \max(1 \cdot C, \lceil \frac{32}{C} \rceil \cdot C)$
Linear Projection	$F_6^{[\text{Lin}]}(X_I) = \text{Conv1d}_{[C \rightarrow n_6]}(X_I^\top, 1, 0, 0, 1)^\top$	$n_6 = 8$	$n_6 = 32$
Identity	$F_7^{[\text{Id}]}(X_I) = X_I$	$n_7 = C$	$n_7 = C$
Embedding	$F_8^{[\text{Emb}]}(X_I) = \mathcal{W}^{[\text{Emb}]}$	$n_8 = 4$	$n_8 = 16$

D. Additional Experiment Results

Table 7. Full MTSF results with forecasting horizons $L_P \in \{96, 192, 336, 720\}$. The best and second best results are in bold and underlined, respectively. Since CATS operates under the same experimental conditions as the models listed in the table, the results for baseline models are obtained from previous literature or from additional experiments conducted for datasets not reported in their literature. A last-value repeat strategy (naive model) is also included for comparison. For input length L_I , CATS and ARM are fixed at 720, while other models select the best result from $L_I \in \{96, 192, 336, 720\}$ as their final result.

Models	CATS (2L)		ARM		PatchTST		DLinear		FEDformer		Autoformer		Informer		Repeat	
	MSE	MAE	MSE	MAE	MSE	MAE	MSE	MAE	MSE	MAE	MSE	MAE	MSE	MAE	MSE	MAE
Electricity (96)	0.125	0.223	0.125	0.222	0.129	0.222	0.140	0.237	0.193	0.308	0.201	0.317	0.274	0.368	1.588	0.946
Electricity (192)	0.142	0.241	0.142	0.239	0.147	0.240	0.153	0.249	0.201	0.315	0.222	0.334	0.296	0.386	1.595	0.950
Electricity (336)	0.155	0.253	0.154	0.251	0.163	0.259	0.169	0.267	0.214	0.329	0.231	0.338	0.300	0.394	1.617	0.961
Electricity (720)	0.174	0.273	0.179	0.275	0.197	0.290	0.203	0.301	0.246	0.355	0.254	0.361	0.373	0.439	1.647	0.975
ETtm1 (96)	0.282	0.339	0.287	0.340	0.293	0.346	0.299	0.343	0.326	0.390	0.510	0.492	0.626	0.560	1.214	0.665
ETtm1 (192)	0.324	0.363	0.328	0.364	0.333	0.370	0.335	0.365	0.365	0.415	0.514	0.495	0.725	0.619	1.261	0.690
ETtm1 (336)	0.358	0.382	0.364	0.384	0.369	0.392	0.369	0.386	0.392	0.425	0.510	0.492	1.005	0.741	1.283	0.707
ETtm1 (720)	0.414	0.416	0.411	0.412	0.416	0.420	0.425	0.421	0.446	0.458	0.527	0.493	1.133	0.845	1.319	0.729
ETtm2 (96)	0.158	0.248	0.163	0.254	0.166	0.256	0.167	0.260	0.203	0.287	0.255	0.339	0.365	0.453	0.266	0.328
ETtm2 (192)	0.211	0.285	0.218	0.290	0.223	0.296	0.224	0.303	0.269	0.328	0.281	0.340	0.533	0.563	0.340	0.371
ETtm2 (336)	0.264	0.322	0.265	0.324	0.274	0.329	0.281	0.342	0.325	0.366	0.339	0.372	1.363	0.887	0.412	0.410
ETtm2 (720)	0.340	0.371	0.357	0.382	0.362	0.385	0.397	0.421	0.421	0.415	0.422	0.419	3.379	1.388	0.521	0.465
ETTh1 (96)	0.365	0.396	0.366	0.391	0.370	0.400	0.375	0.399	0.376	0.415	0.435	0.446	0.941	0.769	1.295	0.713
ETTh1 (192)	0.404	0.420	0.402	0.421	0.413	0.429	0.405	0.416	0.423	0.446	0.456	0.457	1.007	0.786	1.325	0.733
ETTh1 (336)	0.423	0.437	0.421	0.431	0.422	0.440	0.439	0.443	0.444	0.462	0.486	0.487	1.038	0.784	1.323	0.744
ETTh1 (720)	0.441	0.465	0.437	0.459	0.447	0.468	0.472	0.490	0.469	0.492	0.515	0.517	1.144	0.857	1.339	0.756
ETTh2 (96)	0.259	0.327	0.264	0.327	0.274	0.337	0.289	0.353	0.332	0.374	0.332	0.368	1.549	0.952	0.432	0.422
ETTh2 (192)	0.309	0.368	0.327	0.374	0.341	0.382	0.383	0.418	0.407	0.446	0.426	0.434	3.792	1.542	0.534	0.473
ETTh2 (336)	0.329	0.383	0.356	0.393	0.329	0.384	0.448	0.465	0.400	0.447	0.477	0.479	4.215	1.642	0.591	0.508
ETTh2 (720)	0.358	0.415	0.371	0.408	0.379	0.422	0.605	0.551	0.412	0.469	0.453	0.490	3.656	1.619	0.588	0.517
Weather (96)	0.138	0.191	0.144	0.193	0.149	0.198	0.176	0.237	0.217	0.296	0.266	0.336	0.300	0.384	0.259	0.254
Weather (192)	0.182	0.233	0.189	0.240	0.194	0.241	0.220	0.282	0.276	0.336	0.307	0.367	0.598	0.544	0.309	0.292
Weather (336)	0.230	0.274	0.232	0.280	0.245	0.282	0.265	0.319	0.339	0.380	0.359	0.395	0.578	0.523	0.377	0.338
Weather (720)	0.289	0.326	0.296	0.332	0.314	0.334	0.323	0.362	0.403	0.428	0.419	0.428	1.059	0.741	0.465	0.394
Traffic (96)	0.347	0.243	0.356	0.247	0.360	0.249	0.410	0.282	0.587	0.366	0.613	0.388	0.719	0.391	2.723	1.079
Traffic (192)	0.368	0.256	0.373	0.258	0.379	0.256	0.423	0.287	0.604	0.373	0.616	0.382	0.696	0.379	2.756	1.087
Traffic (336)	0.379	0.272	0.383	0.274	0.392	0.264	0.436	0.296	0.621	0.383	0.622	0.337	0.777	0.420	2.791	1.095
Traffic (720)	0.421	0.297	0.425	0.294	0.432	0.286	0.466	0.315	0.626	0.382	0.660	0.408	0.864	0.472	2.811	1.097
Exchange (96)	0.077	0.195	0.078	0.197	0.087	0.207	0.081	0.203	0.148	0.278	0.197	0.323	0.847	0.752	0.081	0.196
Exchange (192)	0.157	0.281	0.150	0.280	0.194	0.316	0.157	0.293	0.271	0.380	0.300	0.369	1.204	0.895	0.167	0.289
Exchange (336)	0.261	0.374	0.252	0.367	0.351	0.432	0.305	0.414	0.460	0.500	0.509	0.524	1.672	1.036	0.305	0.396
Exchange (720)	0.509	0.542	0.486	0.535	0.867	0.697	0.643	0.601	1.195	0.841	1.447	0.941	2.478	1.310	0.823	0.681
Multi (96)	0.022	0.092	0.032	0.125	0.072	0.202	0.067	0.190	0.117	0.261	0.162	0.313	0.092	0.219	0.068	0.189
Multi (192)	0.055	0.146	0.063	0.173	0.167	0.294	0.137	0.269	0.204	0.330	0.356	0.459	0.207	0.338	0.143	0.273
Multi (336)	0.155	0.282	0.164	0.286	0.314	0.405	0.238	0.355	0.313	0.402	0.572	0.705	0.284	0.414	0.264	0.369
Multi (720)	0.419	0.464	0.450	0.503	0.700	0.588	0.476	0.522	0.580	0.544	0.705	0.621	0.921	0.795	0.617	0.551

Table 8. Extended MTSF results on datasets with strong inter-series relationship ($L_P \in \{96, 192, 336, 720\}$). The construction method of MultiX datasets is detailed in section A. For input length L_I , CATS and ARM are fixed at 720, while other models select the best result from $L_I \in \{336, 720\}$ as their final result. The best and second best results are highlighted in bold and underlined, respectively.

Models	CATS (2L)		ARM		PatchTST		DLinear		FEDformer		Autoformer		Informer		Repeat	
	MSE	MAE	MSE	MAE	MSE	MAE	MSE	MAE	MSE	MAE	MSE	MAE	MSE	MAE	MSE	MAE
Multi20 (96)	0.003	0.042	0.005	0.051	0.014	0.091	0.013	0.088	0.033	0.130	0.038	0.151	0.015	0.089	0.014	0.091
Multi20 (192)	0.011	0.077	0.014	0.091	0.023	0.119	0.022	0.112	0.036	0.138	0.044	0.158	0.040	0.151	0.025	0.121
Multi20 (336)	0.015	0.091	0.020	0.110	0.027	0.129	0.027	0.124	0.053	0.171	0.055	0.168	0.086	0.201	0.032	0.138
Multi20 (720)	0.038	0.122	0.035	0.145	0.045	0.164	0.038	0.149	0.109	0.258	0.093	0.237	0.198	0.354	0.044	0.165
Multi50 (96)	0.004	0.045	0.007	0.061	0.014	0.092	0.013	0.089	0.031	0.128	0.037	0.151	0.017	0.094	0.014	0.091
Multi50 (192)	0.009	0.070	0.014	0.093	0.024	0.119	0.022	0.114	0.040	0.145	0.039	0.144	0.050	0.156	0.025	0.121
Multi50 (336)	0.018	0.097	0.021	0.113	0.028	0.131	0.027	0.123	0.048	0.161	0.046	0.158	0.144	0.325	0.032	0.139
Multi50 (720)	0.042	0.157	0.040	0.155	0.046	0.165	0.037	0.146	0.120	0.275	0.166	0.348	0.203	0.377	0.044	0.165
Multi100 (96)	0.003	0.043	0.006	0.058	0.014	0.092	0.014	0.089	0.032	0.129	0.038	0.143	0.019	0.099	0.014	0.091
Multi100 (192)	0.008	0.066	0.014	0.091	0.024	0.120	0.022	0.114	0.038	0.142	0.037	0.139	0.046	0.153	0.025	0.121
Multi100 (336)	0.016	0.092	0.021	0.115	0.028	0.131	0.027	0.123	0.050	0.165	0.046	0.154	0.140	0.318	0.032	0.139
Multi100 (720)	0.045	0.168	0.040	0.154	0.046	0.165	0.038	0.148	0.114	0.267	0.356	0.536	0.243	0.424	0.045	0.165
Multi200 (96)	0.003	0.039	0.009	0.075	0.013	0.088	0.014	0.091	0.034	0.133	0.030	0.133	0.014	0.088	0.015	0.092
Multi200 (192)	0.009	0.067	0.017	0.102	0.024	0.118	0.024	0.118	0.038	0.141	0.040	0.145	0.028	0.115	0.026	0.123
Multi200 (336)	0.010	0.102	0.023	0.118	0.027	0.126	0.028	0.127	0.055	0.175	0.084	0.225	0.043	0.155	0.033	0.141
Multi200 (720)	0.044	0.161	0.043	0.160	0.046	0.164	0.037	0.147	0.134	0.294	0.133	0.290	0.241	0.444	0.045	0.166

Table 9. Results of utilizing CATS with different time series predictors. Input length L_I are fixed as 720. The training strategies of last-value demeaning and random dropping are applied to all the baseline models. Better results are highlighted in bold.

Models	2L		2L+CATS		DLinear		DLinear+CATS		Autoformer		Autoformer+CATS		IndLin		IndLin+CATS		Mean		Mean+CATS	
Metric	MSE	MAE	MSE	MAE	MSE	MAE	MSE	MAE	MSE	MAE	MSE	MAE	MSE	MAE	MSE	MAE	MSE	MAE	MSE	MAE
Multi (96)	0.082	0.209	0.022	0.092	0.070	0.193	0.024	0.073	0.345	0.427	0.034	0.119	0.066	0.187	0.015	0.064	0.439	0.488	0.054	0.175
Multi (192)	0.183	0.311	0.055	0.146	0.148	0.279	0.069	0.173	0.475	0.507	0.097	0.230	0.147	0.273	0.048	0.128	0.520	0.528	0.095	0.231
Multi (336)	0.357	0.426	0.155	0.282	0.276	0.379	0.176	0.292	0.613	0.585	0.253	0.384	0.283	0.376	0.140	0.232	0.647	0.581	0.188	0.322
Multi (720)	0.819	0.643	0.419	0.464	0.649	0.561	0.453	0.510	0.948	0.741	0.472	0.510	0.668	0.567	0.469	0.465	1.008	0.704	0.655	0.602
ETTh2 (96)	0.275	0.336	0.259	0.327	0.270	0.341	0.267	0.338	0.363	0.410	0.304	0.373	0.279	0.342	0.273	0.339	0.388	0.425	0.322	0.386
ETTh2 (192)	0.345	0.381	0.309	0.368	0.331	0.375	0.326	0.379	0.381	0.423	0.345	0.398	0.335	0.378	0.329	0.379	0.403	0.434	0.372	0.416
ETTh2 (336)	0.372	0.405	0.329	0.383	0.370	0.401	0.363	0.408	0.384	0.434	0.364	0.411	0.365	0.405	0.367	0.406	0.406	0.438	0.391	0.430
ETTh2 (720)	0.398	0.433	0.358	0.415	0.394	0.434	0.383	0.432	0.433	0.474	0.389	0.447	0.381	0.423	0.374	0.427	0.434	0.461	0.426	0.456

Table 10. Results of the ablation studies of the three ATS principles and OTS shortcut. Input length L_I are fixed as 720. The training strategies of last-value demeaning and random dropping are applied to all the models. The best and second best results are highlighted in bold and underlined, respectively.

Models	CATS (2L)		w/o Continuity		w/o Sparsity (Channel)		w/o Sparsity (Temporal)		w/o Sparsity (Full)		w/o Variability (Pure Linear)		w/o Variability (Pure Conv)		w/o OTS Shortcut	
Metric	MSE	MAE	MSE	MAE	MSE	MAE	MSE	MAE	MSE	MAE	MSE	MAE	MSE	MAE	MSE	MAE
Multi (96)	0.022	<u>0.092</u>	0.031	0.122	0.026	0.091	0.028	0.107	0.035	0.107	0.043	0.151	0.035	0.126	<u>0.024</u>	0.099
Multi (192)	0.055	0.146	0.081	0.197	0.089	0.191	0.074	0.178	0.082	0.195	0.096	0.217	0.089	0.210	<u>0.058</u>	<u>0.153</u>
Multi (336)	0.155	0.282	<u>0.178</u>	<u>0.285</u>	0.195	0.302	0.202	0.303	0.183	0.294	0.217	0.336	0.186	0.302	0.191	0.293
Multi (720)	0.419	0.464	0.634	0.566	0.710	0.570	0.519	0.573	0.731	0.600	0.595	0.563	<u>0.485</u>	<u>0.497</u>	0.562	0.523
ETTh2 (96)	0.259	0.327	0.263	<u>0.329</u>	0.267	0.334	<u>0.261</u>	<u>0.329</u>	0.270	0.338	0.265	0.330	0.266	0.334	0.288	0.353
ETTh2 (192)	0.309	0.368	<u>0.317</u>	0.371	0.324	0.373	0.320	0.373	0.328	0.377	<u>0.317</u>	<u>0.370</u>	0.323	0.373	0.334	0.387
ETTh2 (336)	0.329	0.383	<u>0.338</u>	<u>0.392</u>	0.342	0.393	0.349	0.397	0.351	0.399	0.346	0.393	0.344	0.394	0.369	0.411
ETTh2 (720)	0.358	0.415	0.381	0.426	<u>0.362</u>	0.451	0.376	0.423	0.372	<u>0.421</u>	0.379	0.426	0.375	0.424	0.384	0.433

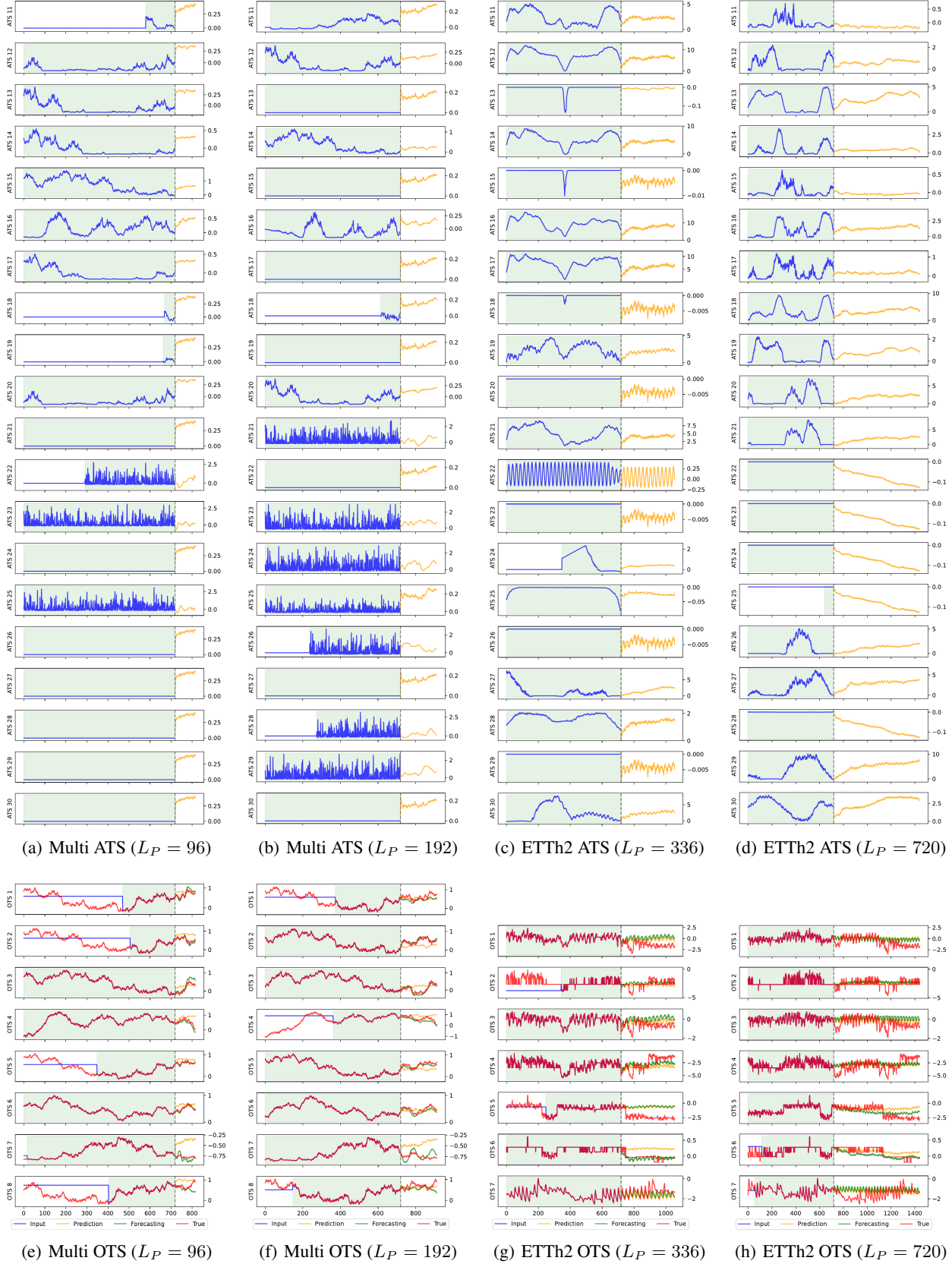


Figure 7. Visualization of CATS (2L) results for the Multi and ETTh2 datasets with one example datapoint for each plot. 20 selected ATS (A^{11} to A^{30}) and all the OTS are displayed. The red line represents the ground truth for each OTS channel. The blue line shows the predictor input for each ATS/OTS channel. **The yellow line indicates the ATS/OTS prediction. The green line is the final forecasting results, combining ATS and OTS predictions.** In the input domain, we use a green box to highlight the area remained after the temporal sparsity cutoff. Note that many input channels are turned into horizontal lines, which is caused by channel sparsity suppressing them; these series still have output prediction due to the bias in the 2L MLP. Full visualization can be found in supplementary materials.